Renewable Energy 81 (2015) 509–522

Contents lists available at ScienceDirect

Renewable Energy

journal homepage: www.elsevier.com/locate/renene

Development of a composite sea wall wave energy converter system

Mariano Buccino [a], Dimitris Stagonas [b], Diego Vicinanza [c, *]

[a] Department of Civil, Architectural and Environmental Engineering, University of Naples Federico II, Via Clauio 21, Naples, Italy
[b] Dept of Civil, Environ & Geomatic Eng, Faculty of Engineering Science, University College London, Gower Street, London, WC1E 6BT, UK
[c] Dipartimento di Ingegneria Civile, Design, Edilizia e Ambiente, Seconda Università degli Studi di Napoli, Via Roma 29, 81031 Aversa (Caserta), Italy

ARTICLE INFO

Article history:
Received 26 July 2014
Accepted 5 March 2015
Available online 8 April 2015

Keywords:
Wave energy
Low-head hydropower
Shoreline wave energy converter
Composite seawall

ABSTRACT

The cost-effective utilization of wave energy is still a major engineering challenge. Shoreline locations for Wave Energy Converters (WECs) offer lower wave energy densities when compared with offshore locations, but give significant advantages from the points of view of construction, maintenance and grid connection.

This article provides a first analysis on the viability of a very low-head hydropower plant, in which waves accumulate water into a shoreline reservoir created by a steep detached ramp. The system is particularly suitable for micro-tidal environments such as the Mediterranean Sea and has the additional advantage of protecting shorelines, seawalls and coastal assets from wave action.

Physical model tests, conducted with regular waves, have been used to get a preliminary estimate of the average water flux overtopping the ramp in a sea state; a novel low-head hydropower machine, developed at Southampton University, has been considered for the conversion of the hydraulic energy into electricity.

The site of Porto Alabe, located along the West coast of Sardinia (Italy), has been chosen as a first case study. Based on the inshore wave climate, the layout of the ramp has been designed as a tradeoff between the needs of maximizing the energy production, providing the coastal area with an adequate protection and making the plant a desirable investment to either private or public players. The results are interesting both from a technical and an economic point of views and encourage a further deepening on the response of this kind of WEC.

1. Introduction

Europe is a frontrunner in the research, development and deployment of ocean energy technologies and a considerable effort has been devoted to assess wave energy availability along and offshore the European coastline [1–4]. Of particular interest for the present work is the area of the Mediterranean Sea, which has a deep water annual average resource of about 30 GW [5].

Marine renewable energy installations might provide substantial benefits to the economies of coastal areas [6], but their success strongly depends on the development of wave energy converters (WECs), which are efficient and cost effective [7–13].

As of today more than 1000 WECs have been patented worldwide, which can be roughly divided into three groups based on the working principle [5]. In the *Oscillating Water Column* technology (OWC), a cushion of air is trapped within a partly submerged chamber where the water level rises and falls with the waves. The oscillating motion makes the air to pass through a turbine, which rotates in the same direction irrespective of the way of flow. An array of such converters is currently being tested in a breakwater in Mutriku/Spain [14].

Wave Activated Bodies (WAB) exploit the relative motion of the different parts of the device; hydraulic systems are generally employed to compress oil, air or water, which are then used to drive a generator.

In the OverTopping Devices (OTD), a sloping plate leads the waves to overtop into a reservoir. The energy is then extracted via a turbine that works with small head differences (below 3 m) and large flow volumes. Several OTDs have been developed so far, such

* Corresponding author. Tel.: +39 3284820770.
E-mail address: diego.vicinanza@unina2.it (D. Vicinanza).

http://dx.doi.org/10.1016/j.renene.2015.03.010
0960-1481/

as the pioneering Tapchan (Tapered Channel Wave Power Device [15]), the floating device "Wave Dragon" [10] and the Seawave Slot-cone Generator (SSG, [16,17]), which employs a number of reservoirs placed on the top of each other.

WECs can be also classified as offshore, nearshore or shoreline devices, depending on their depth of placement. An interesting comparison of the performances of five different technologies in the Portuguese nearshore area has been recently provided by Refs. [18]; in this paper, instead, the focus is on shoreline devices.

The utilization of wave energy at the shoreline is very attractive from the point of view of construction, access, maintenance and grid connection, but also poses difficult problems. Firstly, the available wave energy at the shoreline is lower than the offshore wave energy, although a recent work demonstrated that the reduction of the technically usable resource is not that significant [13]. Secondly, the device is exposed to very intense loadings generated by breaking waves.

Many shoreline systems were designed in the past, based on both the OWC and the overtopping principles. Among the OTDs, a prototype of the aforementioned "Tapchan" deserves to be recalled; the device consisted of a concentrating channel, where incoming waves increased their height prior to spill into a reservoir from which a turbine was driven [14]. Built in 1985 at Toftestallen (Norway), the WEC had been working for several years.

In this paper a different approach is considered, which uses a shoreline reservoir created by a short and steep detached ramp designed to be overtopped by waves (Fig. 1).

The system, conceptually similar to stilling basins and composite seawalls [19–21], offers itself as a multi-purpose structure for wave energy utilization and coastal defense and is particularly suited to micro-tidal environments such as the Mediterranean Sea. Here, the rocky coasts are also provided with a shore plateau just below the mean water level, which reduces the construction efforts.

The reason why shoreline basins have drawn little attention so far, is the lack of a cost-effective turbine that can exploit the "ultra low-head" source of hydropower supplied by the tank (head differences below 2 m). Recently however a low cost technology (called *Hydrostatic Power Machine*, HPM) was developed at and demonstrated by Southampton University; this has then encouraged a deeper investigation into the potential of the system.

The work is organized as follows. The Section 2 analyzes the overtopping performances of smooth nearshore ramps through the results of physical model tests specifically conducted at the University of Southampton. The Hydrostatic Power Machine is presented Section 3. In the Section 4, the application of the conversion system to a site of the West Sardinia (Italy) is studied both from the technical and the economic point of views.

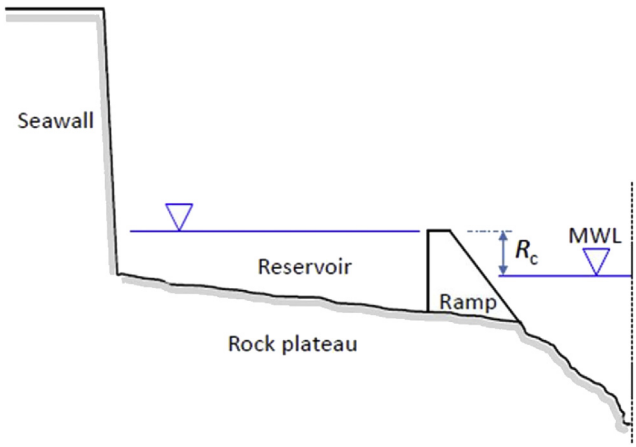

Fig. 1. Sketch of a shoreline reservoir.

2. Overtopping rates for low crested nearshore ramps

Despite wave overtopping represents one of the most researched topics of maritime and coastal engineering, the case of steep low crested nearshore ramps has not been studied in sufficient detail so far. As noticed in Refs. [22], the reason of this lack of knowledge lies in the fact that traditional engineering had actually no interest in structures which produce a large amount of overtopping. Thus, since the response of the outer ramp is obviously central to the performance of the WEC here discussed, an array of ninety 2D physical model tests were specifically carried out at the University of Southampton (*UoS*).

The experiments were conducted with regular waves, as the latter pose the simplest forcing condition possible and allow for a more direct comprehension of the wave–structure interaction.

Regular wave results will be assumed preliminary valid also for random waves. This hypothesis, which is physically justified by the narrow bandedness of sea wave spectra, has been empirically verified in literature for a number of processes even of non linear nature, such as wave breaking [23], wave reflection [24] and wave transmission [25].

Since the present study aims at a first analysis on the viability of the "stilling basin" conversion system, the above equivalence can be considered of course reasonable. For further refinements, however, random wave experiments are indeed necessary.

The following sections describe the experimental set-up and compare tests outcomes to the predictive tools suggested in literature.

2.1. Experiments description

Two series of experiments were performed, with scale ratios of 1:50 and 1:23 respectively. The former (Fig. 2a) was conducted in a flume 8 m long and 0.3 m wide, with a water depth at the wave-maker of 0.13 m. The latter (Fig. 2b) was carried out in a channel that measured 12 m in length and 0.4 m in width; the offshore water depth was 0.255 m.

In both cases *multi-sloped* (composite) *ramps* were tested, because, as discussed in the Section 2.4, they may represent an interesting trade-off between the needs of a structure relatively mild (which increases the rate of overtopping) and reducing the construction costs. The small scale structure encompassed a first segment inclined 1:2, followed by a stretch sloping 1:1. In the 1:23 experiments, the lower part of the ramp was instead inclined by 1:2.6.

For each test series two different crest freeboards (R_c) were used, corresponding to 1.0 and 1.5 m at full scale. The incident wave heights at the toe of the ramps, H_t, had prototype values ranging between 0.71 and 2.5 m; the wave periods, T, varied in the interval 3.5 s − 10 s.

Each experiment lasted for 10 wave cycles; the mean overtopping rate was estimated dividing the volume of water collected in the reservoir behind the slopes (Fig. 2) by the duration of the tests. Because the latter was rather short, the water depth at the toe of the ramps, and accordingly the crest freeboards of the structures, could be considered constant in time.

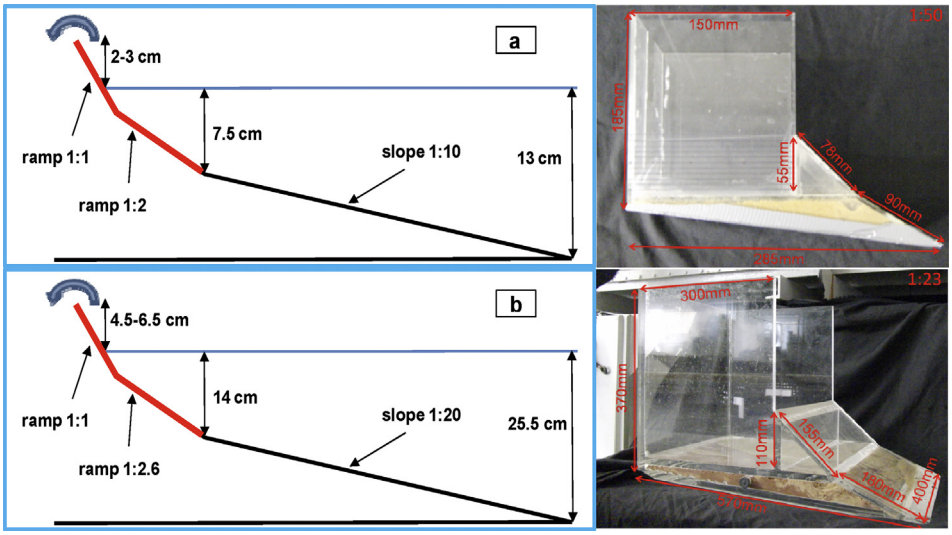

Fig. 2. Sketch of the models.

2.2. Scale effects

Since all model structures and slopes were smooth and impermeable (made of Perspex), scale effects are not supposed to significantly affect the overtopping rate, except for the influence of the surface tension. Nonetheless, as it was initially suggested in Ref. [26] and later confirmed in Refs. [27], the effects of the latter can be neglected if, as in the *UoS* experiments, the water depth at the toe of the structure is larger than 0.02 m and the wave period is longer than 0.35 s.

It might be also of interest to briefly discuss on the effects of wave breaking [26]. noticed that the energy globally dissipated in the process (which has actually an influence on the amount of overtopping) remains in similitude even at small scales, although the internal details of the flow may change; this concept was later corroborated by the experiments of [28]. However, as far as the present tests are concerned, only non breaking waves or surging breakers with a very small bubbling area [29] were observed, owing to both the incident wave characteristics and the steep face of the ramps. This obviously renders the role of wave breaking in fact secondary.

On the other hand, the occurrence of breaking onto the front face of a WEC would lead to a significant loss of the energy available for conversion and accordingly should be prevented for a number of sea conditions as high as possible.

2.3. Prediction tools for the mean overtopping discharge at smooth slopes

As mentioned before, wave overtopping is a topic researched for a long time. In particular over the course of the last decade substantial advancements have come from the EC research project *CLASH* [30], as well as from several national programs. The *EurOtop Manual* [31] takes account the new results and provides an useful guide for practical applications. Among the outcomes of the intense research activity described above, a big deal of design tools have been proposed to calculate the mean overtopping discharge *per* unit of width (q) at different types of structures. Some of them are briefly reviewed below, with respect to the case of smooth and impermeable straight (simple) slopes subjected to head-on random waves.

In the early eighties [32], the following empirical formula was proposed, which is recommended by the *British guidelines*:

$$\frac{q}{\left(g\,H_{1/3,t}T_m\right)} = a\,exp\left(-\,b\,\frac{R_c}{T_m\sqrt{g\,H_{1/3,t}}}\right) \tag{1}$$

where $H_{1/3,t}$ is the statistically defined incident significant wave height at the toe of the slope, R_c is the crest freeboard, T_m is the mean zero-crossing period and a and b are constant parameters related to the front slope angle.

A different expression has been suggested in the framework of the *CLASH* project, starting from previous research by Ref. [33] and based on the results of new experiments:

$$q^* = \frac{q}{\sqrt{\left(g\,H_{m0t}^3\right)}} = min\begin{cases}\dfrac{0.067}{\sqrt{tan\alpha_s}}\,\xi_{-10}\,exp\left(-\,\dfrac{4.75}{\xi_{-10}}\,\dfrac{R_c}{H_{m0t}}\right)\\ 0.2\,\exp\left(-\,2.6\,\dfrac{R_c}{H_{m0t}}\right)\end{cases} \tag{2}$$

where g is the gravity acceleration, H_{m0t} is the spectral significant wave height at the toe of the slope, $tan\alpha_s$ is the inclination of the slope and $\xi_{-10} = tan\alpha_s/(H_{m0t}\,2\pi/g\,T_{-10}^2)$ is the *Iribarren* number based on the mean spectral period T_{-10} [34].

It is noteworthy that for steep slopes, such as those used in the *UoS* experiments, the overtopping discharge is invariably given by the second of the previous relationships, which is worldwide known as the *van der Meer and Janssen formula*.

To quantify the uncertainty related to Eq. (2), the coefficients 4.75 and 2.6 can be considered as normally distributed random variables, with standard deviations equal to 0.5 and 0.35, respectively.

[35] argued that the *CLASH* formula neglects both the effects of the local water depth (h_t) and of the seabed inclination ($tan\vartheta$) and proposed the following:

$$q^* = exp\left[-\left(A + B\,\frac{R_c}{H_{m0,t}}\right)\right] \tag{3}$$

in which:

$$\begin{cases} A = A_0 \ tanh\left[(0.956 + 4.44\ tan\theta)\left(\dfrac{h_t}{H_{m0t}} + 1.242 - 2.32\ tan^{0.25}\theta\right)\right] \\ B = B_0 \ tanh\left[(0.082 - 2.22\ tan\theta)\left(\dfrac{h_t}{H_{m0t}} + 0.578 + 2.32\ tan\theta\right)\right] \end{cases} \quad (4)$$

and

$$\begin{cases} A_0 = 3.4 - 0.734\ cot\alpha_s + 0.239\ cot^2\alpha_s - 0.0162\ cot^3\alpha_s \\ B_0 = 2.3 - 0.5\ cot\alpha_s + 0.15\ cot^2\alpha_s - 0.011\ cot^3\alpha_s \end{cases} \quad (5)$$

The formula is valid for:

$$\begin{cases} 0 \le cot\alpha_s \le 7.0 \\ 0 \le \dfrac{h_t}{H_{m0,t}} \le 23 \end{cases} \quad (6)$$

and the ratio between measured and predicted non dimensional discharges is expected to lie within the range:

$$\left(q^*_{pred}\right)^{2/5} \le \frac{q^*_{meas}}{q^*_{pred}} \le \left(q^*_{pred}\right)^{-\frac{1}{3}} \quad (7)$$

with, $q^*_{pred} \le 1$.

Further to the above mentioned empirical formulae, which have been developed for conventional coastal structures [36], suggested the following equation for OTDs with a single reservoir:

$$q^* = (\lambda_{dr}\lambda_{\alpha s}\lambda_{rc})0.2\ \exp\left(-2.6\ \frac{R_c}{H_{m0,t}}\right) \quad (8)$$

where the parameters $\lambda_{dr.}$, $\lambda_{\alpha s}$ and λ_{rc} respectively account for the effects of waves passing under floating devices ($\lambda_{dr} = 1$ here), of the front slope angle and of the low-crestedness of the structure. $\lambda_{\alpha s}$ and λ_{rc} are given by:

$$\lambda_{\alpha s} = cos^3(\alpha_s - 30^\circ) \quad (9)$$

$$\lambda_{rc} = \begin{cases} 0.40\ sin\left(0.667\pi\ \dfrac{R_c}{H_{m0,t}}\right) + 0.60 \quad for\ \dfrac{R_c}{H_{m0,t}} \le 0.75 \\ 1 \quad for\ \dfrac{R_c}{H_{m0,t}} > 0.75 \end{cases} \quad (10)$$

Eq. (8), is valid for $0.58 \le \cot\alpha_s \le 2.75$ and $0.15 \le R_c/H_{m0,t} \le 2$.

Recently [22], conducted extended tests with random waves and proposed a set of predictive equations specifically for steep, straight, low-crested ramps. In contradiction to *UoS* experiments, all slopes investigated in Ref. [22] were located in relatively deep waters ($h_t/H_{m0,t} > 2.5$). For $\cot\alpha_s \le 1.50$, the authors found the following expressions:

$$q^* = \begin{cases} (0.033\ cot\alpha_s + 0.062)exp\left[(1.08\ cot\alpha_s - 3.45)\dfrac{R_c}{H_{m0t}}\right] \\ 0.2\ \exp\left[(1.57 cot\alpha_s - 4.88)\dfrac{R_c}{H_{m0t}}\right] \end{cases} \quad (11)$$

The first of the above formulae is valid for $0 \le R_c/H_{m0t} \le 0.8$, whereas the second is valid for $0.8 \le R_c/H_{m0t} \le 2.0$. The 90% confidence bands are $(q^*)_{meas.}/(q^*)_{pred.} = 10^{\pm 0.099}$ for $0 \le R_c/H_{m0t} \le 0.8$ and $10^{\pm 0.165}$ for $0.8 \le R_c/H_{m0t} \le 2.0$.

An alternative predictor for the mean overtopping discharge, is the *Delft Hydraulics Artificial Neural Network* [37]. The latter (referred to as *ANN* hereafter) was developed in the framework of the *CLASH* project and provides the expected value of q and the correspondent variation interval for a large variety of structural geometries and wave conditions. It is valid for:

$$\begin{cases} 0 \le cot\alpha_s \le 10 \\ 0.005 \le s_{m-10} \le 0.07 \\ 0 \le R_c/H_{m0t} \le 6.4 \end{cases} \quad (12)$$

where s_{m-10} is the mean wave steepness calculated **with** $T_{m-10.}$

2.4. Comparison of experimental results with prediction model

2.4.1. The approach

The most suited prediction method for calculating the overtopping discharge at the nearshore ramp is here selected by comparing random wave predictors and regular wave experimental data. The boundaries within which this approach can be considered acceptable have been already outlined at the beginning of this chapter. According to [38], it is though necessary to clearly establish which wave parameters (wave height and period) have to be used for the comparison to be physically consistent.

In this regard, the analysis has revealed a substantial independence of data on the wave period; on one side this simplifies the problem as allows eliminating one parameter. On the other side, the result also leads to exclude the Eq. (1) from comparison, since it would suffer, obviously, from an inherent lack of fit.

As for the wave height, in principle two criteria may be followed depending on the context of application; one assumes regular and irregular waves to have the same energy, which implies that the regular wave height, H_t, equals the root mean square wave height, H_{rms}, of the random sea-state (see for example [39] and [40]). The other presupposes the two trains possesses the same characteristic wave height, in this case $H_t = H_{m0t}$.

An accurate inspection of the physical structure of the Eqs. (2,3,8 and 11) suggests the latter to be the most appropriate. Since the overtopping rate is made non dimensional through the variable $(gH^3_{m0t})^{0.5}$, the quantity at the right hand side of the formulae can be interpreted as the discharge coefficient of an ideal weir with a water level on the crest equal to H_{m0t}. Consequently, the water level being equal (i.e. if $H_t = H_{m0t}$), the flow rate is expected to be approximately the same, although the energies of the random and periodic wave trains differ by a factor of 2. The reasoning is assumed to hold also for the Neural Network.

On the other hand, the "energetic equivalence" would imply that many waves in the irregular wave train are higher than H_t; since high waves are the most significant for the overtopping process, this seems of course unreasonable.

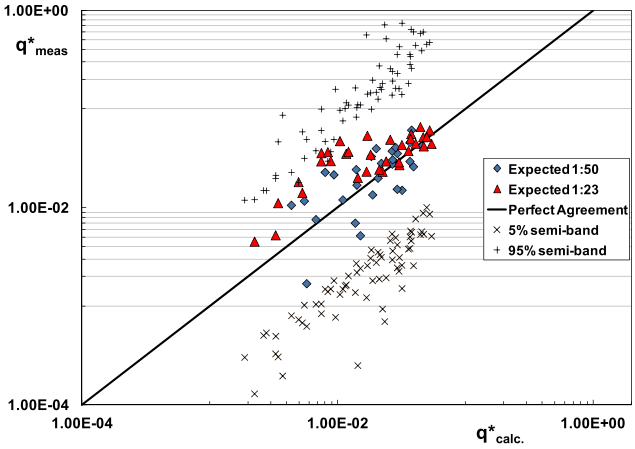

Fig. 3. Experimental data vs. predictions of ANN.

2.4.2. Quantitative comparison

For a quantitative comparison, it should be remembered that all the design tools here considered were developed for simple (straight) slopes; thus, for composite structures like those tested at *UoS*, a mean value of the inclination has to be employed.

On the basis of physical arguments about the position of the breaking point along the ramp [31], recommends using, as first estimate, the average between the points located at $\pm 1.5\ H_{m0t}$ about MWL. If $+1.5\ H_{m0t}$ is located above the crest, then R_c should be taken as the reference point. This mean angle, which will be referred to as $\alpha_{s,eq}$ hereafter, is also incorporated in the ANN.

The predictions of the Neural Network, along with the confidence bands at the 90% probability level, are compared with the experimental data in Fig. 3. The comparison is presented in terms of non dimensional "weir-like" discharge $q^* = q/(gH_t^3)^{0.5}$.

The overall agreement is reasonable; the confidence bands are not exceeded, but span 2 or 3 orders of magnitude, indicating that the overtopping process inherently produces a remarkable scatter.

In presence of such a big variance, it is more convenient to assess the performances of the predictive models via the "*geometric mean*" and "*geometric standard deviation*" introduced by Ref. [35]. They are defined as follows:

$$\begin{cases} X_G = exp\left\{\dfrac{1}{N}\sum_1^N \ln x_i\right\} \\ \sigma(X_G) = exp\left\{\left[\dfrac{1}{N}\sum_1^N\left(\ln^2 x_i - \ln^2 X_G\right)\right]^{0.5}\right\} \end{cases} \tag{13}$$

where $x_i = q^*_{meas.}/q^*_{pred.}$

X_G values larger (smaller) than 1 reveal a tendency to overestimate (underestimate) the experimental results, whilst $\sigma(X_G)$ represents the number by which $q^*_{pred.}$ should be multiplied and divided with, in order to acquire the variation of measurements around predictions.

Table 1
Reliability indexes for the overtopping predictors.

Predictive tool	Equation#	Tests 1:50		Tests 1:23	
		X_G	$\sigma(X_G)$	X_G	$\sigma(X_G)$
ANN	–	0.913	1.756	0.560	1.725
EUROTOP	(2)	0.995	1.401	0.470	1.778
GODA	(4)	0.610	1.493	0.307	1.607
KOFOED	(8)	0.937	1.389	0.447	1.808
VITOR & TROCH	(11)	0.662	1.351	0.272	2.332

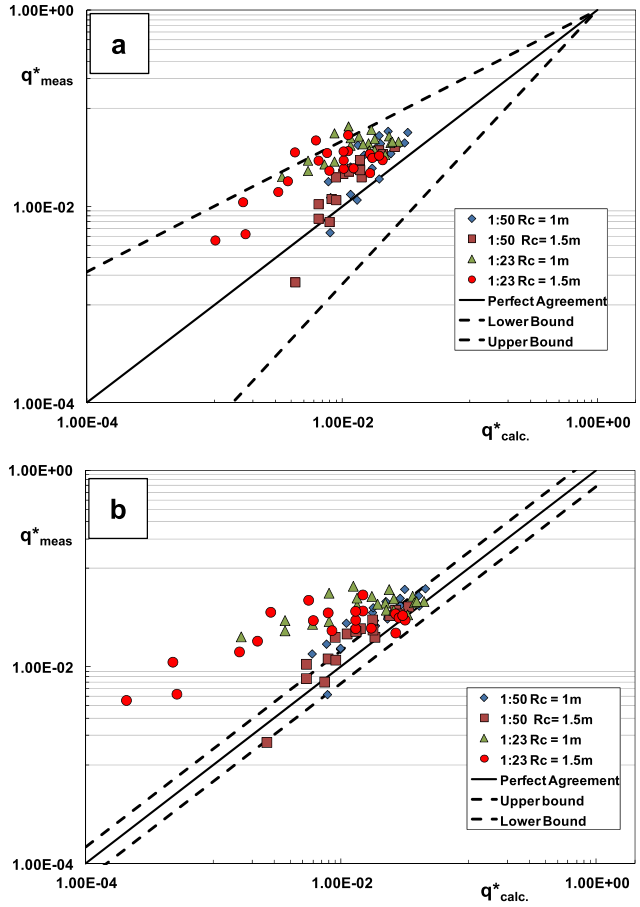

Fig. 4. Panel a): experimental data vs. Eq. (3); Panel b): experimental data vs. Eq. (11).

Table 1 summarizes the values of the above indexes for all the design tools except Eq. (1).

All the models are able to capture the order of magnitude of the measured discharges and this empirically confirms, as a whole, the argument of the equivalence (at a first approximation level) between regular and random wave experiments with $H_t = H_{m0t}$.

However, the predictions are systematically more accurate for the smaller scale, while 1:23 data are underestimated by a factor included between 1.8 and 3.7. Eq. (3) and Eq. (11) provide the worst fit, but the former (Fig. 4a) has the 95% of points lying within the variation bands of Eq. (7); otherwise, Eq. (11) returns large errors on 1:23, remaining the small scale results basically on the inside of the confidence intervals or very close to them (Fig. 4b).

Since scale effects are likely negligible (as discussed in the Section 2.2), the underprediction of 1:23 data may be due to the fact that $\alpha_{s,eq}$ does not allow to properly account for the effect of the milder 1:2.6 underwater slope; as waves do not break on the ramps, the latter is in fact expected to increase the potential run up and then the overtopping rate. In this regard, it is also worth noticing that the absence of breaking on the structure renders the use of $\alpha_{s,eq}$ questionable in itself.

Accordingly, a new definition for the average slope value is introduced here. As the majority of tests were conducted with 'low crest conditions' ($R_c/H_t \leq 1.2$) it can be assumed that the part of the slope above the MWL has limited influence on overtopping. As such, the new average slope value ($\alpha_{sb,eq}$) is calculated from the following:

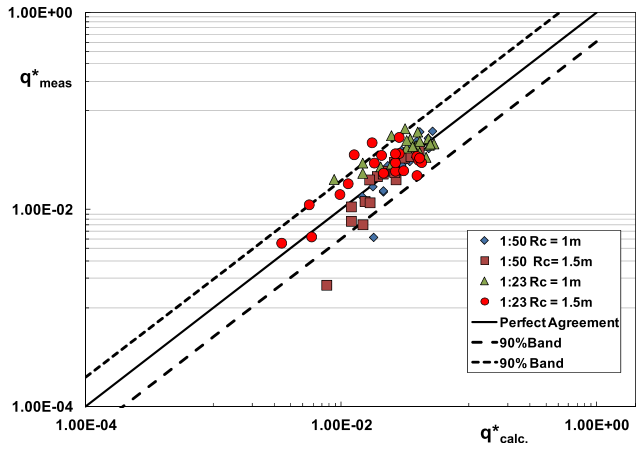

Fig. 5. Experimental data vs. Eq. (11) after using Eq. (14). The 90% bands are given by ± exp(1.64 ln(σ(X$_G$))).

$$cot\left(\alpha_{sb,eq}\right) = \frac{l_{sub}}{h_{sub}} \tag{14}$$

where l_{sub} and h_{sub} are the length and height of the submerged part of the structure, respectively.

When using $\alpha_{sb,eq}$, the quality of the estimates has been seen to improve for all the predictive tools; in particular Eq. (11) fits the data rather well (Fig. 5), giving an overall X_G of 1.08 and a $\sigma(X_G)$ of 1.51. Furthermore, the model proved to be robust also for $\cot(\alpha_{sb,eq}) = 1.85$, that is slightly beyond the upper limit value 1.5 suggested for simple slopes.

A satisfactory agreement ($X_G = 1.02$; $\sigma(X_G) = 1.45$) was also obtained with the Eq. (8), once the coefficient 2.6 has been replaced with the formula:

$$min\left[2.63; 0.1776\exp\left(4.1972\ tan\ \alpha_{sb,\ eq.}\right)\right] \tag{15}$$

The comparison with data is shown in Fig. 6. Eq. (15) holds for $\tan(\alpha_{sb,eq}) > 0.53$ and yields a value of 2.63 for slopes steeper than 0.65.

In principle the dependence of the overtopping rate on the "submerged slope angle" appears interesting, as the possibility of shortening the emerged part of the structures without a loss of discharge can lead to a reduction of construction costs. However, supplementary experiments are needed to validate the correctness of previous results and establish their application range.

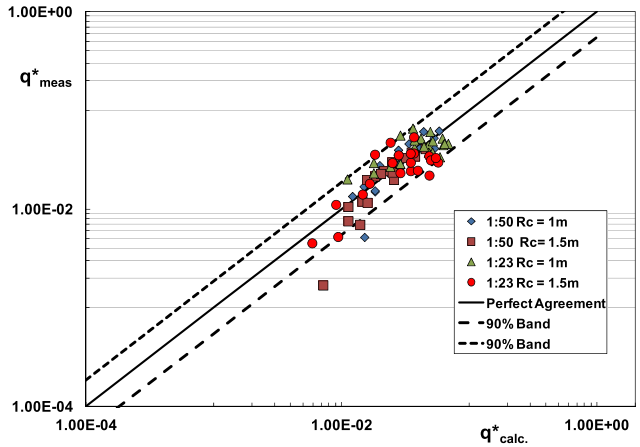

Fig. 6. Experimental data vs. Eq. (8) after using Eq. (15). The 90% bands are given by ± exp(1.64 ln(σ(X$_G$))).

In the calculations presented in the Section 4 the predictions of the Eq. (11) will be employed. This basically for two reasons; one is that it required no variation of the parameters (once the proper mean angle has been introduced), which indicates a good robustness. The other is that the formula was originally derived for smooth low crested overtopping ramps similar to those examined here, although located in deeper waters.

Nevertheless, some discussion on the effects of using a different equation for the overtopping rate is given in the Sections 4.3 and 4.5.

3. Ultra low-head hydropower converter: the Hydrostatic Pressure Machine (HPM)

The cost-effective utilization of hydropower with very low head differences (say less than 2.5 m) is still a problem, since standard turbine technologies may result quite expensive [41]. compared different types of hydropower converters and argued that the cost of the double regulated machine, associated with the need of structures for both minimizing the inflow losses and decelerating the outflowing water (thereby recovering the pressure head), render Kaplan turbines not cost effective in most cases (see also [42]).

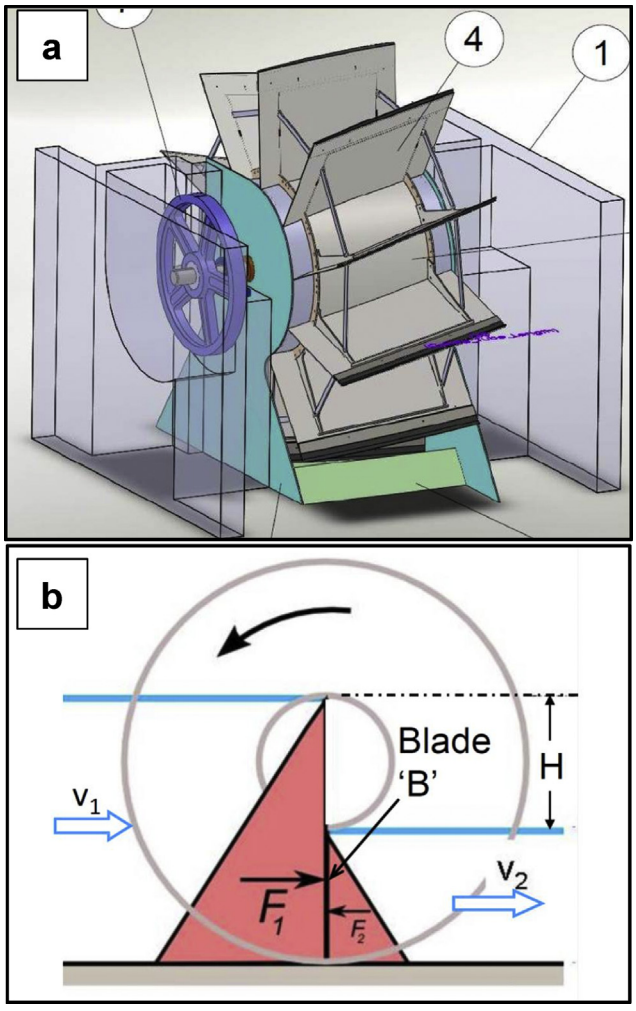

Fig. 7. The Hydrostatic Power Machine: a. Isometric view; b. Principle.

Accordingly, an alternative low cost turbine – the Hydrostatic Pressure Machine (HPM) – is herein considered.

The HPM, developed within the EC funded research project *Hylow*, consists of a hub with a diameter close to the head difference and 10–12 blades which close the downstream from the upstream water level. At the bed, the blades run in a curved section with the length of one blade distance – the shoe – to minimize leakage losses. The hydrostatic pressure difference resulting from the different water levels acts on the blades and provides the driving force. Fig. 7a and b show the principle of the HPM and an isometric view.

The HPM was developed for head differences between 1 and 2.5 m, with flow volumes of 1–3.5 m^3/s/m and power outputs of 6–52 kW/m. Flow volume and power output increase with increasing head difference. In the frame of *Hylow*, the theory of the machine was developed [43] and full scale tests on a 6 kW (el.) prototype with a head difference of 1.2 m were conducted. Based on prototype and large scale model test results [44,45], and assuming a downstream water level at the bottom of the hub, an idealized total efficiency curve (hydraulic to grid including all losses) was derived with a maximum efficiency of 68% for a ratio of flow rate Q and design flow rate Q_{Des} of $Q/Q_{Des} = 0.41$ (Fig. 8). The efficiency then decreases to 0.66 for $Q/Q_{Des} = 0.635$ and to 0.56 for $Q/Q_{Des} = 1.0$.

The HPM was found to be cost effective, with overall costs of 7200 €/kW installed capacity for the 6 kW prototype. The large cells and slow speed of the machine (2–12 rpm) resulted in good ecological characteristics.

4. Application to a case study

To explore the potential of a shoreline reservoir coupled with *HPM*, a site located along the North West coast of Sardinia (Italy) has been selected as a case study.

4.1. Site description

The North West Sardinian coast, around the town of Alghero (Fig. 9), is the most resourced of the whole Italy; owing to the development of large convective systems caused by fronts of cold air coming from the Atlantic Ocean, intense thunderstorms take place, which tend to merge into Mesoscale Convective Systems (MCS). The latter have a metereological scale larger than the individual thunderstorms and are capable of generating severe sea-states, which persist for several hours.

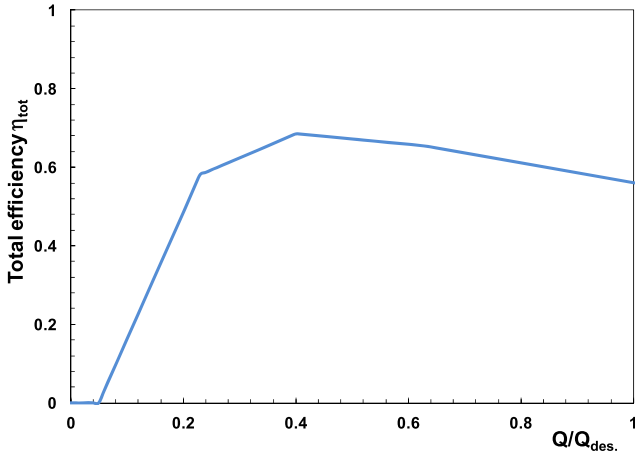

Fig. 8. Idealized total efficiency curve of HPM.

In addition to being energetically resourced, the area features a rocky coastline and a plateau just below the MWL, all suitable characteristics for the construction of a shoreline tank.

4.2. Wave climate

Using extensive buoy records and hindcast data [47], estimated the offshore yearly average wave power in the area around Alghero at about 10 kW/m, the bulk of which is supplied by north–westerly waves. The mean monthly availability is approximately 15 kW/m in the period November–February whereas it drops to about 5 kW/m during the cooling season (May–August). On the whole, the threshold of 10 kW/m is exceeded continuously from November–April and this makes the area one of the most energetic of the Mediterranean Sea.

The offshore wave climate has been then propagated to the −20 m bathymetric line and the nearshore potential of the 7 points labeled with the codes "S1–S7" in Fig. 10 has been assessed.

In the following the point S6 (Porto Alabe) is used as reference, essentially because of the high power available (10.91 kW/m, with a mean yearly energy of 96 MWh/m). Table 2 reports the inshore wave climate of the site for directional sectors of 30°. The tide levels have been found to be included between −0.9 m and +0.3 m.

It is worth mentioning that a wave power availability of the order of 10 kW/m (say between 10 and 20 kW/m) is typical of the European coast facing the North Sea [48]. This includes the Eastern shores of UK, the most Southern part of the Norvegian coasts, the coasts of the Netherlands and Belgium and shores of Denmark. Accordingly, the results presented below may apply also to those areas, provided that the characteristics of the coastline are suited to the installation of a shoreline reservoir. Nevertheless, as will be shown in the next section, the effectiveness of the plant could be severely affected by the local tide height.

4.3. The hydraulic energy available

For a given ramp layout, the amount of hydraulic energy available per year and per meter of structure width ($E_{hyd.}$ in MWh/m) can be calculated as follows:

$$E_{hyd} = 0.00876 \sum_{td,min}^{td,\,max} \sum_{\beta=-90^\circ}^{+90^\circ} \sum_{Hmin}^{Hmax} \rho g q\left(H, \beta, \alpha_{sb,eq.},\ R_c^{td},\ td\right) R_c^{td} \times \Delta f(H, \beta,\ td) \tag{16}$$

in which:

I. the overtopping rate q (in m^3/s/m) is calculated through Eq. (11);
II. the crest freeboard R^{td}_c (in m) is relative to the tide level "*td*";
III. ρ is the water density (kg/m^3) and
IV. Δf indicates the relative frequency of occurrence, i.e. the ratio between the number of hours in which a given climate condition has been observed and the duration (in hours) of the total observation period (see Table 2).

Both q and Δf are function of the angle of propagation of waves relative to the normal to the coastline β (in degrees); [49], suggests to include this parameter in the overtopping discharge formulae by dividing the relative crest freeboard (R_c/H_{m0t}) with a correction factor (γ_β), the expression of which has been originally proposed in Ref. [36]:

$$\gamma_\beta = \max(1 - 0.0033|\beta|; 0.736) \tag{17}$$

Fig. 9. The isle of Sardinia and the town of Alghero (source: [35]).

For all calculations, the wave parameters of Table 2 have been re-arranged using directional sub-sectors of 5°N and each class of wave height and wave angle has been substituted with the corresponding average value. It should also be noted that due to the extremely steep foreshore characterising the site (mean slopes of about 1:2.5 between −20 m and −5 m), the effects of both shoaling-refraction and wave breaking have been tentatively neglected. This appears reasonable because most of waves reach the very shallow water area in less than one wavelength (see Table 2), while the breaking index tends to become very high; for example according to [23] one would get:

$$\left(\frac{H}{h}\right)_b = 0.56 \cdot exp\left(\frac{3.5}{2.5}\right) = 2.27 \tag{18}$$

Furthermore, a simplified approach has been adopted to account for tide; the range −0.9 m/+0.3 m has been divided into 5 equiprobable classes of 0.24 m range, which have been supposed to be statistically independent of H and β. Thus, one gets:

$$\Delta f(H, \beta, td) = \Delta\varphi(H, \beta) \cdot 0.2 \tag{19}$$

where $\Delta\varphi(H,\beta)$ is the joint frequency of occurrence of wave height and wave direction; the tide levels used in the calculations (td) correspond to the midpoints of the classes. Fig. 11, illustrates the calculated hydraulic energy plotted over the crest height relative to the MWL (R_{cMWL}) and as a function of $\cot(\alpha_{sb,eq})$. The computation has been carried out using a step of 0.1 m. For a given ramp slope, the curves exhibit a maximum, say $(E_{hyd})_{max}$, generated by the product of q, which decreases with the crest freeboard, times R_c. As $\cot(\alpha_{sb,eq})$ grows from 1 to 1.9, $(E_{hyd})_{max}$ more than doubles, passing from nearly 16.8 MWh/m–36.4 MWh/m; at the same time, the value of R_{cMWL} at the peak of energy raises from 1.1 m to 1.8 m.

The effect of using a different overtopping predictor is shown in Fig. 12 with reference to the Equations (2) and (8). The maximum energy available is some less compared with Fig. 11, being nearly 33 MWh/m for Eqs. (2) and (28) MWh/m for Eq. (8). The major differences are though detected with respect to the role of the ramp slope; the latter is in fact not considered in Eq. (2), whereas in the Eq. (8) there would be no effects for $\cot(\alpha_{sb,eq}) > 1.6$. Note that in both cases more energy would be available on steeper ramps, implying a possible reduction of the plant costs; as an example, Eq. (8) predicts $(E_{hyd})_{max} = 25.54$ MWh/m for 1:1, whereas with Eq. (11) the same level is achieved only with a 1.5 (i.e. 50% longer) slope.

Although for the rest of the article the Eq. (11) will be employing (extended to slopes milder than 1.5 in agreement with empirical findings of Section 2), the discussion above clearly highlights how the development of a reliable overtopping formula for the near-shore ramps would be meaningful to the future research works on this kind of WEC.

It is now of interest to investigate how tide levels may affect the performances of the wall. Thus, for the same wave climate 8 symmetric tide ranges have been considered, which increase from ±0 m (no tide) to ±3.5 m at a step of 0.5 m. The effect on $(E_{hyd})_{max}$ is displayed in Fig. 13 for three values of the front slope angle. The "solid-pointed" curves describe the variation of the peak energy, whereas the dashed ones refer to the ratio $(E_{hyd})_{max}/(E_{hyd})_{max,no\ tide}$. The maximum hydraulic energy available reduces by 40%–50% at ±3.5 m, with the drop increasing as the slope become steeper; on the other hand, for ±0.5 m the reduction is included between 0.1% and 1.8% and for ±1 m the loss lies in the range 2.8%–7.5%.

The above result is easily explained by the fact that large tidal variations require large values of R_{cMWL} to avoid the ramp to be submerged; this, as qualitatively indicated in Fig. 11, produces a significant reduction of the hydraulic energy available.

This certainly advices against the use of the shoreline basin system in severe tide environments, also considering that large crest freeboards increase the total costs of the plant.

4.4. Power production

The energy produced by the system during an average climatic year is given by:

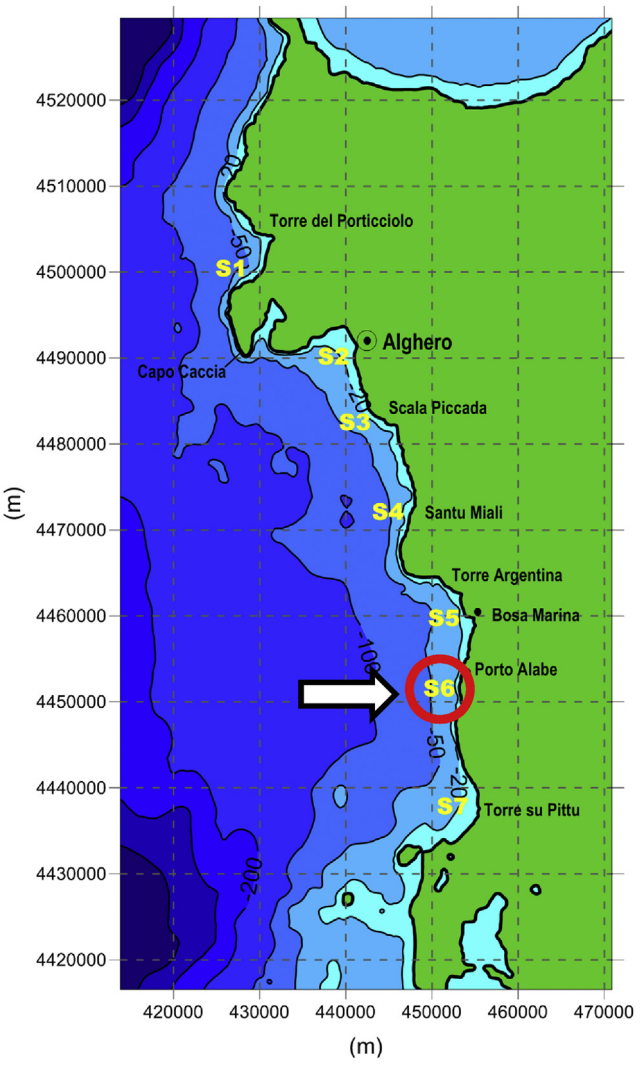

Fig. 10. Location of the nearshore sites. (Source [35]). The site selected for the present study is circled in red. (For interpretation of the references to color in this figure legend, the reader is referred to the web version of this article.)

$$E_P[MWh] = 0.00876 \sum_{td,mim}^{td,max} \sum_{Qmin}^{Qmax} \rho g \cdot Q \cdot R_c^{td} \cdot \eta(Q) \cdot \Delta f(Q,\ td) \tag{20}$$

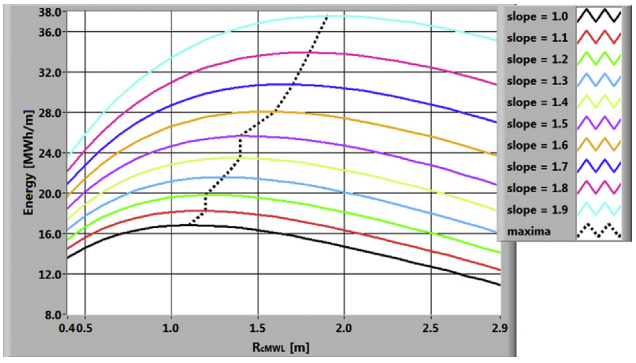

Fig. 11. Hydraulic energy as a function of the crest freeboard and of the front slope angle.

in which, according to the common practice of traditional hydropower plants, the *flow rate used to generate power*, Q, has been assumed to be:

$$Q = \begin{cases} 0, & q \cdot b \le 0.05 Q_{des} \\ Q \cdot b, & 0.05 Q_{des} < q \cdot b < Q_{des} \\ Q_{des}, & Q_{des} \le q \cdot b \le 3 Q_{des} \\ 0, & 3 Q_{des} < q \cdot b \end{cases} \tag{21}$$

where b denotes the alongshore length of the basin and Q_{des} is the "*design flow rate*", which is defined as a value of the mean overtopping discharge ($q \cdot b$) that is exceeded for "t_{des}" days a year. In compliance with Eq. (21), the conversion stops when the flow rate is either very small (less than 5% of Q_{des}) or rather large (more than 3 Q_{des}), whereby in the range Q_{des} − 3 Q_{des} the power is generated using the design discharge.

The efficiency curve of the turbine, $\eta(Q)$, is that depicted in Fig. 8 of Section 3; once the mean crest freeboard and the mean ramp angle have been fixed, the joint frequency of occurrence $\Delta f(Q, td)$ equals $\Delta f(H, \beta, td)$ in Eq. (16).

Altogether E_P depends on 4 variables (Q_{des}, b, $R_{c,MWL}$ and $\alpha_{sb,eq}$), the values of which result from a tradeoff between a number of partially conflicting needs, such as:

- maximizing the production;
- minimizing the cost of the plant;
- maximizing the degree of coastal protection;
- minimizing the intrusion of the structures in the landscape;
- guaranteeing a proper exchange of water between the shoreline basin and the open sea.

Table 2
Inshore wave climate for the site of Porto Alabe (S6). Values indicate the relative frequencies of occurrence.

Direction	H_{m0} [m]	0–0.5	0.5–1.0	1.0–1.5	1.5–2.0	2–2.5	2.5–3.0	3.0–3.5	4.0–4.5	4.5–5.0	5.0–5.5	5.5–6.0	6.0–6.5	6.5–7.0	**Sum**
[°N]	T_{-10}[s]	4.42	5.55	6.42	7.17	7.80	8.73	9.07	9.64	9.90	10.10	10.29	10.60	10.95	
0–30		0	0	0	0	0	0	0	0	0	0	0	0	0	**0**
30–60		0	0	0	0	0	0	0	0	0	0	0	0	0	**0**
60–90		0	0	0	0	0	0	0	0	0	0	0	0	0	**0**
90–120		0	0	0	0	0	0	0	0	0	0	0	0	0	**0**
120–150		0	0	0	0	0	0	0	0	0	0	0	0	0	**0**
150–180		0	0	0	0	0	0	0	0	0	0	0	0	0	**0**
180–210		0	0	0	0	0	0	0	0	0	0	0	0	0	**0**
210–240		0.002	0.000	0.000	0.000	0.000	0.000	0.000	0.000	0.000	0.000	0.000	0.000	0.000	**0.002**
240–270		0.199	0.034	0.010	0.000	0.000	0.000	0.000	0.000	0.000	0.000	0.000	0.000	0.000	**0.243**
270–300		0.061	0.071	0.042	0.019	0.009	0.004	0.002	0.001	0.002	0.002	0.001	0.000	0.000	**0.214**
300–330		0.203	0.083	0.051	0.034	0.039	0.032	0.018	0.014	0.037	0.018	0.010	0.003	0.000	**0.541**
330–360		0	0	0	0	0	0	0	0	0	0	0	0	0	**0**
Sum		**0.465**	**0.188**	**0.102**	**0.053**	**0.048**	**0.036**	**0.020**	**0.016**	**0.039**	**0.020**	**0.010**	**0.003**	**0.000**	**1**

The bold indicates the sum of frequencies.

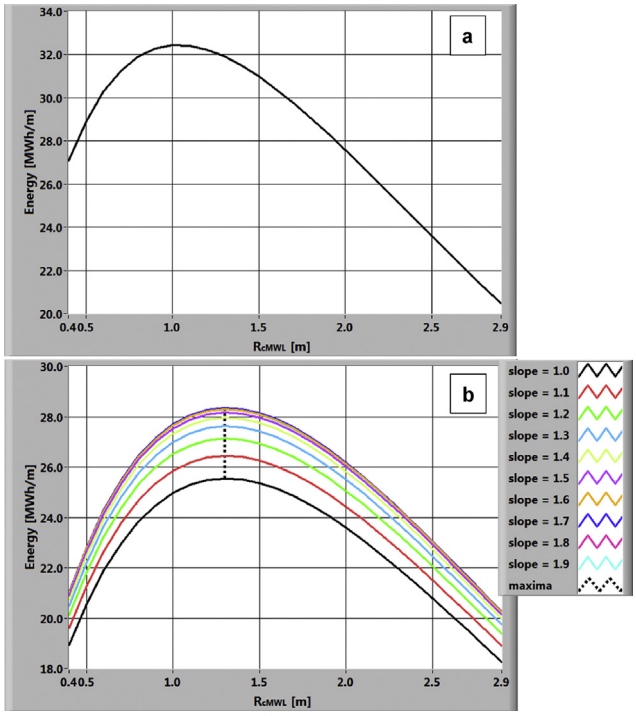

Fig. 12. Calculated hydraulic energy graph after using the Eq. (2), panel a, and the Eq. (8), panel b.

This is a very complex problem where the existence of an absolute optimum is very doubtful.

In the following, a simplified design approach based on a limited number of indicators is presented and discussed.

4.5. Definition of t_{des}

To select t_{des}, two additional parameters over the energy production have been considered. The first is the (*annual*) *plant capacity factor*, C_F, i.e. the ratio between the energy actually produced by the plant (E_P) and the potential output at the full capacity [50]:

$$C_F = \frac{E_P}{8.76 \cdot R} \tag{22}$$

where the rated power, R, equals:

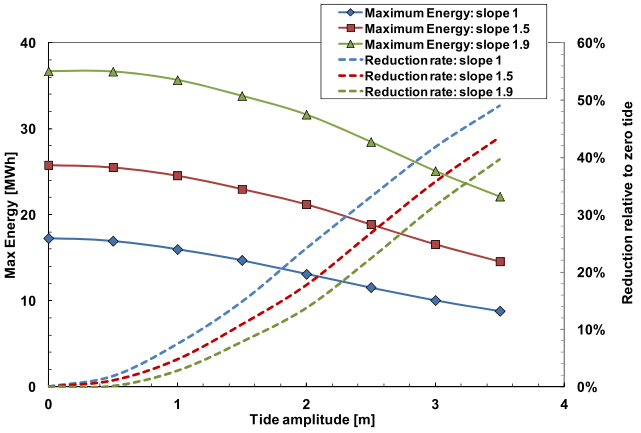

Fig. 13. Max hydraulic energy $(E_{hyd})_{max}$ as a function of the tide amplitude (solid-pointed curves). The dashed lines give the rate of reduction of $(E_{hyd})_{max}$ relative to the case of no tide.

$$R[kW] = 9.81 \cdot Q_{des} \cdot 0.56 \cdot (R_{c,MWL} - td, min) \tag{23}$$

in which *td*, *min* is the average of the lowest tide level class.

In addition, a *working time index* (Wt) has been built, which represents the probability that the overtopping discharge (*qb*) is included between 0.05 Q_{des} and 3 Q_{des}:

$$Wt = \frac{t(0.05\ Q_{des}) - t(3\ Q_{des})}{365} \tag{24}$$

Remembering Eq. (21), Wt basically gives the portion of days in a year in which the turbine produces energy.

In Fig. 14, E_P, C_F and *Wt* are plotted versus $R_{c,MWL}$ for different possible values of t_{des}. The minimum crest freeboard equals 1.3 m to allow the *HPM* to work with an hydraulic head not lower than 1 m (accounting tide). This choice originates from the fact that, as stressed in Section 3, the turbine has been developed and tested for hydraulic heads not lower than 1 m.

Since the results proved independent of both the basin length and the ramp angle, the graph conventionally refers to $b = 10\ m$ and $\cot(\alpha_{sb,eq}) = 1.8$. The panel a) shows that the energy yield

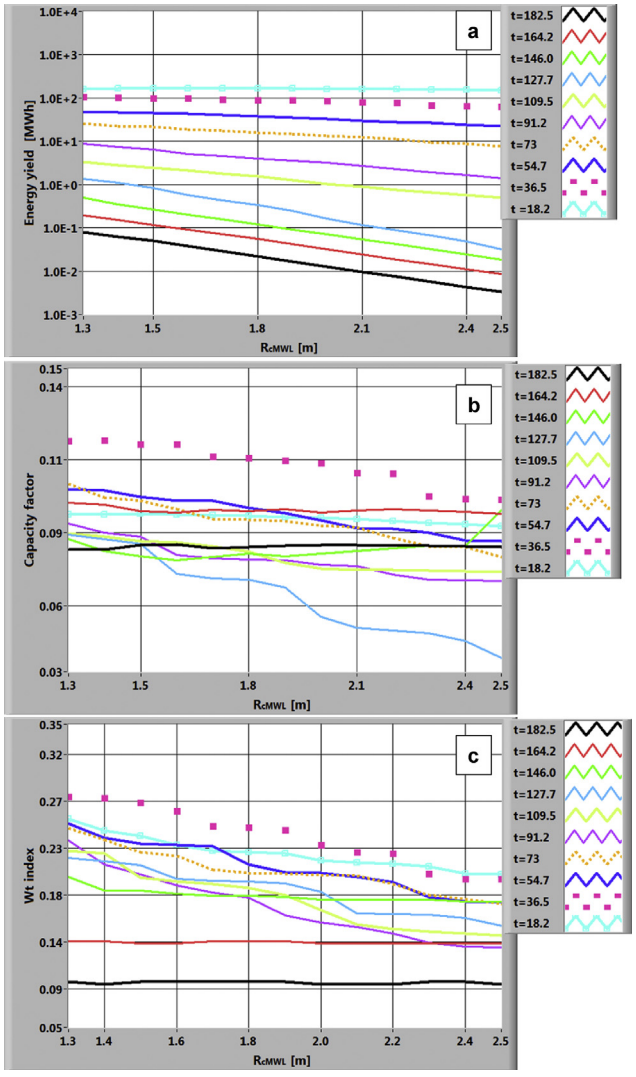

Fig. 14. Energy production (a, in log-scale), capacity factor (b) and working time index (c) as a function of the crest freeboard and of the design period. b = 10 m; $\cot(\alpha_{sb,eq}) = 1.8$.

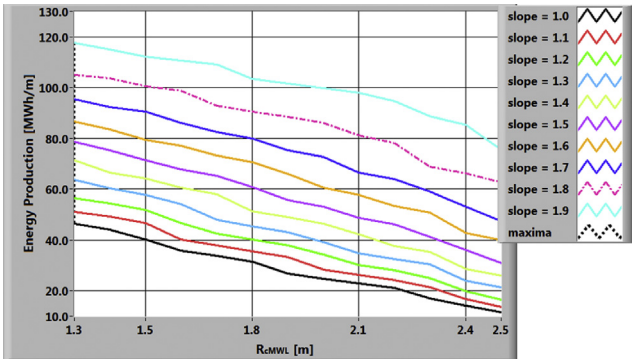

Fig. 15. Energy production for t_{des} = 36.5 days as a function of $R_{c,MWL}$ and for $\cot(\alpha_{sb,eq})$ between 1.0 and 1.9. "b" = 10 m.

monotonically increases as t_{des} reduces; for large time intervals (182.5, 164.2 days) the energy produced is very small, as the waves generated in the majority of the days cause no overtopping unless the outer ramp is extremely low crested.

The design time-interval has been then chosen in correspondence of the maximum of C_F and *Wt*, i.e. at 36.5 days; Fig. 15 displays the energy produced for different values of $\cot(\alpha_{sb,eq})$.

A t_{des} of 36.5 days is unusually small for common hydropower plants and is the consequence of the great uneveness of the wave energy distribution. The capacity factors are also rather low, being of the same order as for solar plants (13.1% on average in Italy); this is partly an effect of the tide, which reduces the time interval in which the maximum power is achieved. Although this is not directly shown here for sake of brevity, it has been found that in absence of tide the capacity factors would have been of the order of 20%, with *Wt* as large as 35%. This gives another example of how negatively a broad variation in the MWL may affect the performance of the system.

It is finally worth mentioning that the results presented above (in terms of t_{des}, C_F and *Wt*) have been found to be only slightly dependent on the overtopping predictor. An example is given in Fig. 16, with respect to the Eq. (8). The optimal t_{des} is the same as when using the Eq. (11) and the maximum values of C_F and *Wt* are only some percentage points lower.

4.6. The design value of $R_{c,MWL}$

The analysis of Fig. 15 suggests choosing a design crest freeboard of 1.3 m; beside maximizing the energy production, and then the reduction of carbon dioxide emissions compared to conventional power plants, this value allows reducing the intrusion of the structure in the coastal landscape and favors the water renewal within the basin.

However, additional design points might be found attempting to balance the needs of high energy yield and effective coastal protection. Assuming that the two requirements are equally important for the local community, and that the effectiveness of coastal protection can be quantified via the transmission coefficient of the outer slope K_t (ratio between the wave heights at rear and in front of the ramp), a simple "*budget function*" may be developed as follows:

$$B_F = \frac{(E_P)_R - (E_P)_{Rmax}}{(E_P)_{Rmax}} + \frac{\left(1-\overline{K_t}\right)_R - \left(1-\overline{K_t}\right)_{Rmax}}{\left(1-\overline{K_t}\right)_{Rmax}} \tag{25}$$

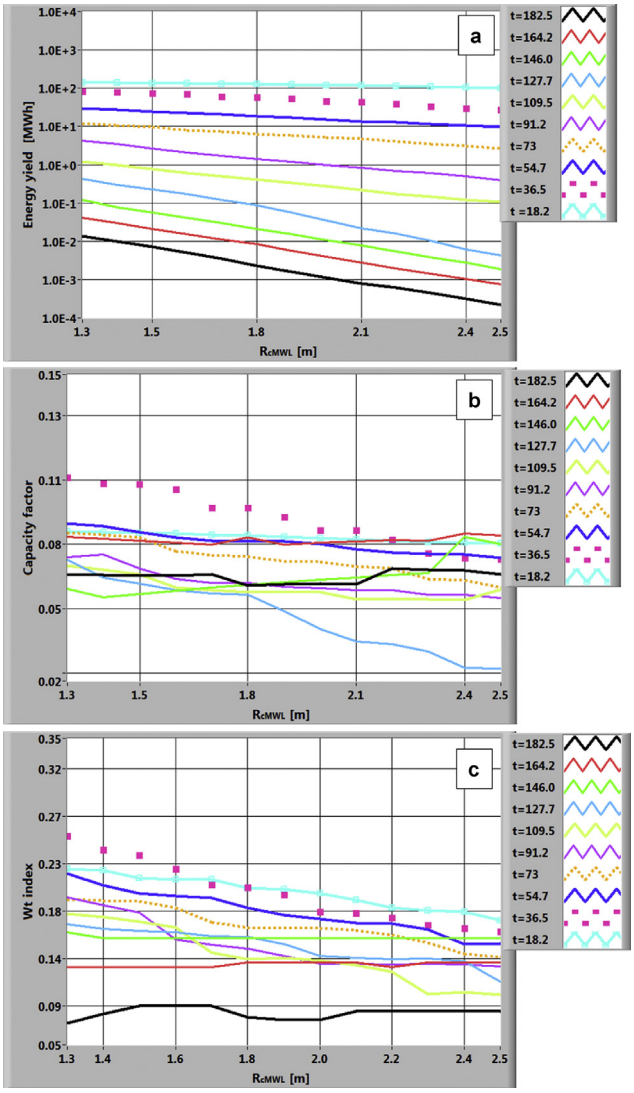

Fig. 16. Energy production plots using Eq. (8) as overtopping predictor. b = 10 m; $\cot(\alpha_{sb,eq})$ = 1.8.

where the subscripts *R* and R_{max} indicates that the quantities are respectively calculated at the generic $R_{c,MWL}$ and at the value of the crest freeboard corresponding to the maximum energy production. B_F is then zero at R_{max}, but might become positive at a different value of $R_{c,MWL}$ if the degree of coastal protection increased percentually more than the loss of E_P.

In the Eq. (23), the overbarred K_t denotes the *yearly averaged transmission coefficient* defined as:

$$\overline{K_t} = \sum_{td,min}^{td,\,max} \sum_{\beta=-90^\circ}^{+90^\circ} \sum_{Hmin}^{Hmax} K_t\left(H, \beta, \alpha_{sb,eq.}, R_c^{td}\right) \cdot \Delta f(H, \beta, td) \tag{26}$$

where the single "instantaneous" K_t equals:

$$K_t\left(H, \beta, \alpha_{sb,eq.}, R_c^{td}\right) = K_{2D}\left(H, \alpha_{sb,eq.}, R_c^{td}\right) \cdot cos^{2/3}\beta \tag{27}$$

in which K_{2D} represents the transmission coefficient under purely bi-dimensional conditions and the correction factor for wave obliquity ($\cos^{2/3}\beta$) is that suggested by Ref. [51]. As far as K_{2D} is concerned, the "conceptual approach" proposed by Ref. [52] has been employed, assimilating the overtopping ramp to a low crested

smooth impermeable breakwater with a zero crown width (triangular barrier). This leads to:

$$K_{2D} = 0.5476 \cdot \sqrt{F\left(\frac{R_c^{td}}{H_{m0t}}\right)} \tag{28}$$

in which F represents the rate of reduction of the overtopping discharge with the relative crest freeboard. In the present case, the comparison with Eq. (11) leads to:

$$F\left(\frac{R_c^{td}}{H}\right) = \begin{cases} exp\left[\left(1.08\, cot\alpha_{sb,\,eq.} - 3.45\right)\frac{R_c^{td}}{H_{m0t}}\right] & for \frac{R_c^{td}}{H_{m0t}} \le 0.8 \\ \exp\left(-4.88\,\frac{R_c^{td}}{H_{m0t}}\right) & for \frac{R_c^{td}}{H_{m0t}} > 0.8 \end{cases} \tag{29}$$

In Fig. 17, the budget function B_F is plotted vs. $R_{c,MWL}$ for values of cot($\alpha_{sb,eq}$) ranging between 1 and 1.9.

The function is always negative and this leads to finally select 1.3 m as design value of the (mean) crest freeboard.

4.7. Choice of basin length and ramp angle

Assuming $t_{des} = 36.5$ days and $R_{c,MWL} = 1.3$ m, the alongshore basin length, b, and the mean slope angle, $cot\alpha_{sb,\,eq.}$, have been determined trying to maximize the financial convenience of the project. Thus a simplified cash-flow analysis has been performed, under the following hypotheses:

- A single *HPM* machine is operating in the basin. This technically limits the rated power of the plant at 100 kW;
- The cost of the turbine has been reasonably estimated through the relationship (Dr. Gerald Muller, personal communication):

$$C_T[€] = (7,429.8 - 38.298\,R)R \tag{30}$$

which returns 7200 €/kW for a rated power of 6 KW (consistently with Section 3) and 3600 €/kW for a rated power of 100 kW;

- The construction cost is 5000 € per meter of basin;
- The cash-in flow is estimated in 300 €/MWh for 15 years. This corresponds to the feed-in tariff offered by the Italian government;
- Maintenance costs are estimated in 7% of the yearly cash-in flow.

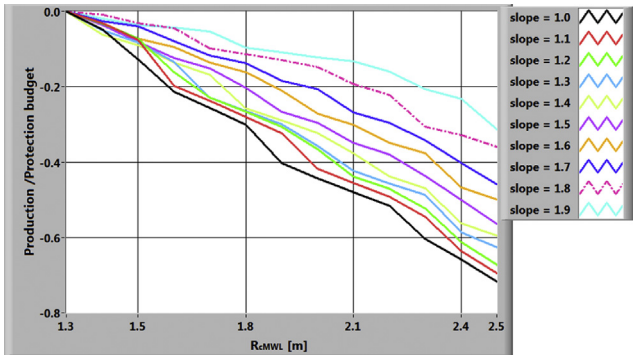

Fig. 17. Budget function (Eq. (23)) for b = 10 m.

Two indicators have been used to assess the performance of the investment, and namely the PayBack Period (*PBP*, i.e. the length of time required to recover the investment) and Mean Annual Interest Rate (MAIR) given by:

$$MAIR\ (\%) = \frac{(15 - PBP)x[Cash - in]}{15xCost\ of\ investment} x100 = \frac{RoI}{15} \tag{31}$$

where *PBP* is expressed in years, [Cash-in] is in Ref. €/year and *RoI* is the Return on Investment.

The financial appeal of the WEC can be conveniently measured by comparing MAIR to the interest rate of the Italian Government Bond with a 15 years duration, BTP-15, which is currently 3.5%. To compensate for all the sources of uncertainty related to the project, especially the use of a design flow rate with a very low exceedance probability (10%), the threshold of desirability of the investment is cautiously set at twice the BTP-15 rate, i.e. 7%.

The Fig. 18 displays, for the usual values of $cot\alpha_{sb,\,eq.}$, the basin length and the *PBP* in function of the rated power, *R*. The payback period decreases linearly for each slope and reduces with $cot\alpha_{sb,\,eq.}$ as a consequence of the fast increment of the produced energy. Similarly, the milder the ramp angle, the lower the basin length required for a given R. Only for $cot\alpha_{sb,\,eq.} \ge 1.5$ the investment can be recovered in a period less than 15 years; in the present study a value of 1.8 is selected to not exceed the maximum value tested within the *UoS* experiments, that is 1.85. The use of a multi linear slope may here contribute to control the costruction costs. For a 100 kW rated power, the basin length required is then approximately 10 m, with a yield of 106.25 MWh per year (*PBP* = 13.71 years).

As it has been designed ($R_c = 1.3$, $cot\alpha_{sb,\,eq.} = 1.8$, $b = 10$ m), the shoreline basin would be able to fulfill the demand of nearly 30 civil houses (3.3 per meter); moreover, according to the Intergovermental Panel on Climate Change 2011, the WEC would lead to a reduction of carbon dioxide emissions of nearly 0.012 tons/year compared to nuclear (generation II) power plants, 0.042 tons/year

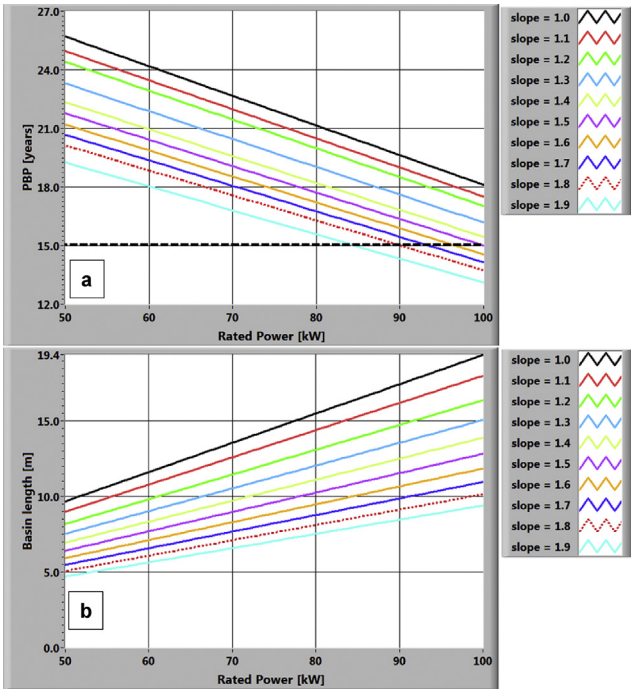

Fig. 18. PayBack Period (a) and basin length (b) as a function of the rated power for $cot\alpha_{sb,\,eq.}$ ranging between 1 and 1.9.

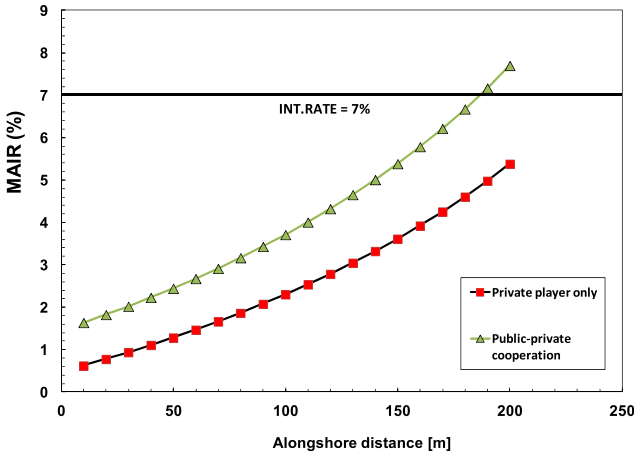

Fig. 19. Interest rate as a function of the alongshore distance covered by WECs.

compared to solar PV, 0.465 tons/year compared to natural gas and 0.996 tons/year compared to a coal p.p.

Yet, the value of *MAIR* (0.62%) is far less than the threshold of 7%. Thus, the investment has to be made desirable through the economies of scale that may arise from supposing that a number of 10 m long basins are constructed alongshore; in this way a sort of low-crested barrier is formed, where several 100 kW machines work independently. In this case it is reasonable to assume a discount for mass production on the turbine cost of 2% for each added machine (up to 20 turbines) and a mean discount on construction works of 2.5% per 100 m constructed.

As shown in Fig. 19 the target would be not reached within the alongshore distance of 200 m, unless a public player (e.g. the City of Porto Alabe or the Region of Sardinia) beared the costs of construction works as a measure for coastal retreat control. In this case a *MAIR* of 7% would be achieved at nearly 190 m (*PBP* = 7.49 years); the public investment of nearly € 770,450, as well as the intrusion of the WEC in the coastal landscape, would be compensated from both the protection guaranteed to the shoreline and the reduction of CO_2 emissions in the atmosphere (nearly 19 tons/year compared to a coal power plant, according to the Intergovermental Panel on Climate Change 2011).

5. Conclusions

The paper has explored the potential of an "ultra-low head" hydropower plant including a shoreline overtopping reservoir, created by a detached low crested ramp, and a novel turbine (the *Hydrostatic Power Machine*) developed to produce energy with head differences ranging between 1 and 3.5 m.

The system, conceptually similar to stilling basins and composite seawalls, offers itself as a multi-purpose structure for wave energy utilization and coastal defense.

The Results of 96 regular wave experiments, specifically conducted at the University of Southampton, have been analyzed to assess the overtopping performance of the outer slope. In the tests, the case of composite (multi-linear) structures has been considered as a possible compromise between the needs of enhancing the overtopping rate and reducing the structure length.

A wide comparison with the predictive tools proposed in literature (Section 2), indicated that conventional formulae for straight structures can be reliably employed as design tools if the average inclination of the submerged part of the ramp is used as equivalent slope. With this adjustment, the Vitor and Troch formula [22] proved to be rather effective; interestingly, the "steep face equations" (Eq. (11)) resulted appropriate even beyond the limit slope of 1.5 suggested by the authors.

The site of Porto Alabe (West Sardinia, Italy) has been selected as a case study. The results of the application can be summarized as follows:

- The great uneveness of wave energy leads to design flow rates with an exceedance time unusually low compared to common hydropower plant;
- The capacity factor ranges between 12% and 20%. These values are of the same order as those of solar PV and wind power plants respectively;
- The presence of severe tides affect negatively both the hydraulic energy available and the capacity factor; this makes this kind of WEC suited to micro-tidal environments, such as the Mediterranean Sea;
- The system seems able to give a remarkable energy yield within a restricted alongshore distance; this mainly because of the role of the slope angle, which would greatly increase the rate of overtopping;
- The heavy uncertainties related to the aforementioned irregularity of the energy input renders the system financially more suited to a collaboration between public and private investors; the function of measure for shore erosion control, however, favors the public intervention, as the defense of the assets from sea flooding events is a primary concern for the coastal communities worldwide.

On the whole, the research outcomes indicate the functioning of the WEC deserves to be further investigated. In particular, future research works should focus on:

- the tweaking of a reliable predictive tool for the overtopping rate of the ramp, based on random wave experiments. As mentioned before, the results of the present study suggest the slope of the structure to be a primary parameter (Figs. 11, 12 and 15), whose role must be carefully investigated;
- the analysis of the effects of wave oscillations on the energy production; the hypothesis of considering only the mean water levels in the calculation of the energy yield needs to be accurately verified, owing to the very low heads the system works at.
- the analysis of the effects of wave breaking, shoaling-refraction and bottom uneveness [53] on the overall efficiency of the system.

Acknowledgments

The research leading to these results has received funding from the European Community's Seventh Framework Programme (FP7/2007-2013) under grant agreement n°212423.

The work also was partially supported by the EC FP7 Marie Curie Actions People, Contract PIRSES-GA-2011-295162 – ENVICOP project (Environmentally Friendly Coastal Protection in a Changing Climate) and by RITMARE Flagship Project (National Research Programmes funded by the Italian Ministry of University and Research). The authors acknowledge Dr Gerald Muller for his most valuable contribution to the development of the original idea and for the fruitful discussions on the details of the application of the HPM.

References

[1] Waters R, Engstrom J, Isberg J, Leijon M. Wave climate off the Swedish west coast. Renew Energy 2009;34(6):1600e6.

[2] Thorpe TW. The wave energy programme in the UK and the European wave energy Network. In: Fourth European wave energy conference, Aalborg (Denmark). Oxfordshire, UK: AEA Technology; October 2000.

[3] Iglesias G, Carballo R. Wave energy resource in the Estaca de Bares area (Spain). Renew Energy 2010;35(7):1574e84.
[4] Guedes Soares C, Rute Bento A, Goncalves M, Silva D, Martinho P. Numerical Evaluation of the wave energy resource along the Atlantic European coast. Comput Geosciences 2014;71:37–49.
[5] Clément A, McCullen P, Falcao A, Fiorentino A, Gardner F, Hammarlund K, et al. Wave energy in Europe: current status and perspectives. Renew Sustain Energy Rev 2002;6(5):405e31.
[6] Azzellino A, Conley D, Vicinanza D, Kofoed JP. Marine renewable energies: perspectives and implications for marine ecosystems. Special Issue Sci World J 2013;2013. ISSN: 1537-744X.
[7] Azzellino A, Ferrante V, Kofoed JP, Lanfredi C, Vicinanza D. Optimal siting of offshore wind-power combined with wave energy through a marine spatial planning approach. Int J Mar Energy 2013;3–4. ISSN: 2214-1669: 11–25.
[8] Carballo R, Iglesias G. Wave farm impact based on realistic wave-WEC interaction. Energy 2013:216–29.
[9] Fernandez H, Iglesias G, Carballo R, Castro A, Fraguela JA, Taveira-Pinto F, et al. The new wave energy converter WaveCat: concept and laboratory tests. Mar Struct 2012;29(1):58–70.
[10] Kofoed JP, Frigaard P, Friis-Madsen E, Sørensen HC. Prototype testing of the wave energy converter wave dragon. Renew Energy 2006;31(2):181–9.
[11] Törnqvist NA. Theoretical analyses of some simple wave power devices. Int J Energy Res 1978;2(3):281–94.
[12] Falcão AFO, Henriques JCC, Cândido JJ. Dynamics and optimization of the OWC spar buoy wave energy converter. Renew Energy 2012;48:369–81.
[13] Folley M, Whittaker TJT. Analysis of the nearshore wave energy resource. Renew Energy 2009;34:1709–15.
[14] Torre-Enciso Y, Ortubia I, Lopez de Aguileta LI, Marques J. Mutriku Wave Power Plant: from the thinking out to the reality [Uppsala, Sweden]. In: EWTEC 2009 proceedings of the 8th European wave and tidal energy conference; 2009.
[15] Falcao AFO. First-generation wave power plants: current status and R&D requirements. J Offshore Mech Arct Eng 2004;126:384.
[16] Buccino M, Vicinanza D, Salerno D, Banfi D, Calabrese M. Nature and Magnitude of wave loadings at Seawave Slot-cone Generators. Ocean Eng 2015;95: 34–58.
[17] Buccino M, Banfi D, Vicinanza D, Calabrese M, Del Giudice G, Carravetta A. Non breaking wave forces at the front face of Seawave Slotcone Generators. Energies 2012;2012(5):4779–803.
[18] Silva D, Rusu E, Guedes Soares A. Evaluation of various technologies for wave energy conversion in the Portuguese nearshore. Energies 2013;2013(6): 1344–64.
[19] Vicinanza D, Contestabile P, Nørgaard J, Lykke Andersen T. Innovative rubble mound breakwaters for overtopping wave energy conversion. Coast Eng 2014;88. ISSN: 0378-3839:154–70.
[20] Geeraert J, De Rouck J. Reduction of wave overtopping at seadikes: stilling wave basin – 3D research. Proc ICCE 2008 2008;4:3157–63.
[21] Mori M, Yamamoto Y, Kimura K. Wave force and stability of upright section of high mound composite seawall. Proc ICCE 2008 2008;4:3164–72.
[22] Victor L, Troch P. Wave overtopping at smooth impermeable steep slopes with low crest freeboards. J Waterw Port Coast Ocean Eng 2012;138:372–85.
[23] Kamphuis JW. Incipient wave breaking. Coast Eng 1991;15:185–203.
[24] Zanuttigh B, van der Meer JW. Wave reflection from coastal structures in design conditions. Coast Eng 2008;55:771–9.
[25] Adams CB, Sonu CJ. Wave transmission across submerged near surface breakwaters. Proc Int Conf Coast Eng 1987:1729–38.
[26] Le Méhauté B. An introduction to hydrodynamics and water waves. New York: Springer; 1976.
[27] Kortenhaus A, van der Meer JW, Burcharth HF, Geeraerts J, van Gent M, Pullen T. Final Report on scale effects. CLASH WP7-report, LWI and Germany. 2004.
[28] Stive MJF. A scale comparison of wave breaking on a beach. Coast Eng 1985;9: 151–8.
[29] Galvin CJ. Breaker type classification on three laboratory beaches. J Geophys Res 1968;73(12):3651–9.
[30] De Rouck J, Verhaeghe H, Geeraerts J. Crest Level Assessment of coastal Structures: general overview. Coast Eng 2009;56(2):99–107.
[31] EurOtop. EurOtop. Wave overtopping of sea defences and related structures: Assessment manual. In: Pullen T, Allsop NWH, Bruce T, Kortenhaus A, Schüttrumpf H, van der Meer JW, editors. Environment Agency, UK/ENW Expertise Netwerk Waterkeren, NL/KFKI Kuratorium für Forschung im Küsteningenieurwesen; 2007. Germany, http://www.overtopping-manual.com. Mar. 11, 2011.
[32] Owen MW. Overtopping of sea defences. In: International conference on the hydraulic modelling of civil engineering structures; 1982. p. 469–80.
[33] van der Meer JW, Janssen JPFM. Wave Run-Up and wave overtopping of dikes. Wave forces on inclined and vertical wall structures. In: Kobayashi N, Demirbilek Z, editors. ASCE; 1994. p. 1–27.
[34] Battjes JA. Surf similarity. In: Proceedings of 14th coastal engineering conference (American Society of civil Engineers); 1974. p. 466–80.
[35] Goda Y. Derivation of unified wave overtopping formulas for seawalls with smooth, impermeable surfaces based on selected CLASH datasets. Coast Eng 2009;56(4):385–99.
[36] Kofoed JP. Wave overtopping of marine structures—Utilization of wave energy. Ph.D. thesis. Aalborg, Denmark: Aalborg Univ; 2002.
[37] van Gent MRA, Van den Boogaard HFP, Pozueta B, Medina JR. Neural network modelling of wave overtopping at coastal structures. Coast Eng 2007;54(8): 586–93.
[38] Thompson EF, Vincent CL. Significant wave height for shallow water design. J Waterw Port Coast Ocean Eng 1985;111(5):828–42.
[39] Battjes JA, Stive MJF. Calibration and verification of a dissipation model for random breaking waves. J Geophys Res 1985;90(C5):9159–67.
[40] Calabrese M, Vicinanza D, Buccino M. 2D wave setup behind low crested and submerged breakwaters. In: Proc International offshore and polar engineering conference; 2003. p. 2176–81.
[41] Bozinhova S, Hecht V, Kisliakov D, Müller G, Schneider S. Hydropower converters with head differences below 2.5 m. In: Proceedings of the Institution of Civil Engineers (ICE). ICE Publishing; 2013. http://dx.doi.org/10.1680/ener.11.00037.
[42] Gieseke J, Jorde K. Technical and economical overall concepts for the reactivation, modernization and relicencing of hydropower plants. In: Proceedings of the 28th IAHR congress; 1999 [Graz, Austria].
[43] Senior J, Saenger N, Müller G. New hydropower converters for very low head differences. J Hydr Res 2010;48(6):703–14.
[44] Stagonas D, Müller G, Maravelakis N, Magagna D, Warbrick D. Composite seawalls for wave energy conversion: 2D experimental results. In: 3rd International Conference on ocean energy, 6 October; 2010 [Bilbao/Spain].
[45] Müller G, Linton N, Schneider S. Das Projekt Hylow: die Wasserdruckmaschine Feldversuche mit einem Prototypen (The project Hylow: The hydrostatic pressure machine, field tests with a prototype, in German). Korresp Wasserwirtsch KW 2012;5(1):22–39.
[46] Schneider S, Müller G, Saenger N, Zanke U. Nutzung von geringen Fallhöhen zur Energiegewinnung – Untersuchungen an einer Wasserdruckmaschine. Korresp Wasserwirtsch 2011;4(6):329–34.
[47] Vicinanza D, Contestabile P, Ferrante V. Wave energy potential in the northwest of Sardinia (Italy). Renew Energy 2013;50. ISSN: 0960-1481:506–21.
[48] Eurowaves project, available at http://www.oceanor.no/projects/eurowaves.
[49] De Waal JP, van der Meer JW. Wave runup and overtopping on coastal dikes. In: Proc. of the international conference on coastal engineering. Venice, Italy: ASCE; 1992. p. 1758–71.
[50] Wadhwa CL. Generation, distribution and utilization of electrical energy. New Age International Ltd Publisher; 2005. p. 365.
[51] van der Meer JW, Briganti R, Zanuttigh B, Wang B. Wave transmission and reflection at low-crested structures: design formulae, oblique wave attack and spectral change. Coast Eng 2005;52(10–11):915–29.
[52] Buccino M, Calabrese M. Conceptual approach for prediction of wave transmission at low-crested breakwaters. J Waterw Port Coast Ocean Eng 2007;133(3):213–24.
[53] Rezanejad K, Bhattacharjee J, Guedes Soares C. Stepped sea bottom effects on the efficiency of nearshore oscillating water column device. Ocean Eng 2013;2013(70):25–38.